Geophysical Research Letters

RESEARCH LETTER
10.1029/2020GL090967

Key Points:

- Quasiperiodic 60 minute Alfvén waves at Saturn can be modeled as field line resonances corresponding to the third and fourth harmonics
- Realistic plasma density and magnetic field models are important for calculation of eigenfrequencies, especially in the outer magnetosphere
- Neither a hydromagnetic box model nor a dipole field approximation is adequate for determining eigenfrequencies in the outer magnetosphere

Supporting Information:

Supporting Information may be found in the online version of this article.

Correspondence to:

L. Rusaitis,
rusaitis@ucla.edu

Citation:

Rusaitis, L., Khurana, K. K., Kivelson, M. G., & Walker, R. J. (2021). Quasiperiodic 1-hour Alfvén wave resonances in Saturn's magnetosphere: Theory for a realistic plasma/field model. *Geophysical Research Letters*, *48*, e2020GL090967. https://doi.org/10.1029/2020GL090967

Received 21 OCT 2020
Accepted 4 FEB 2021

Quasiperiodic 1-Hour Alfvén Wave Resonances in Saturn's Magnetosphere: Theory for a Realistic Plasma/Field Model

L. Rusaitis[1], K. K. Khurana[1], M. G. Kivelson[1,2], and R. J. Walker[1]

[1]Department of Earth, Planetary, and Space Sciences, University of California, Los Angeles, CA, USA, [2]Department of Climate and Space Sciences and Engineering, University of Michigan, Ann Arbor, MI, USA

Abstract We model the omnipresent quasiperiodic 60 min waves in Saturn's outer magnetosphere as field line resonances adopting a realistic magnetic field model and a measurement-based plasma density distribution using Alfvén wave resonance theory for arbitrary field geometries (Singer et al., 1981). The modeled eigenfrequencies for the second and higher modes are roughly independent of invariant latitude, mapping into large regions of the magnetosphere up to at least 20 R_S, and the third and fourth harmonic modes having close to 1 h eigenperiod. The model predicts the normalized amplitudes of these higher modes of the magnetic field perturbations at high latitudes to exceed the amplitudes at the plasma sheet, in agreement with the observations of more frequent occurrences at mid-to-high latitudes. The periods of the higher order field line resonances in the outer magnetosphere differ considerably from those in a dipole model, illustrating the importance of a realistic field model.

Plain Language Summary 1-h waves have been observed around Saturn for a long time, but their origin remains not well understood. We study these waves as resonances of Saturn's magnetic field, in an analogous way to a plucked guitar string vibrating at its natural frequency. One could approximate Saturn's magnetic field as a bar magnet, but we show that such an approximation is not sufficient to reproduce 1 h waves throughout large regions far outside Saturn. Similar to how a guitar's string is dependent on its mass and length, we also use a realistic plasma mass density along the field, and show that the higher harmonics of these vibrations match the observed 1 h wave period.

1. Introduction

One of the more puzzling features in Saturn's magnetosphere is the source of persistent quasiperiodic 60 min (QP60) phenomena, which became particularly apparent during continuous in-situ investigations by the Cassini spacecraft from 2004 to 2017. The QP60 phenomena are observed in much of the magnetospheric data, from magnetic field fluctuations (Bunce et al., 2014; Mitchell et al., 2016; Yates et al., 2016) and field-aligned electron beams and ion conics (Mitchell, Kurth, et al., 2009; Schardt et al., 1985) to auroral pulsations (Bader et al., 2019; Bunce et al., 2014; Menietti et al., 2020; Mitchell, Krimigis, et al., 2009; Mitchell et al., 2016) and auroral hiss (Carbary et al., 2016). An extensive global survey of these events is provided by Roussos et al. (2016) and Palmaerts et al. (2016), focusing both on their spatial and spectral distribution. We will focus on the transverse quasiperiodic magnetic field perturbations in this study.

The QP60 magnetic field oscillations were found mostly in the outer magnetosphere, mapping inside Titan's orbit of roughly 20 R_S (Carbary et al., 2016) and beyond, with highest frequency of occurrence in the dusk sector and mid-to-high latitudes (Roussos et al., 2016). The field perturbations are typically transverse to the magnetic field with amplitudes between 1.0×10^{-1} and 1 nT (Kleindienst et al., 2009; Yates et al., 2016), and come in short wave trains, that is, they typically last ∼5 h before decaying. The Alfvénic signature of these perturbations, as well as the persistence of the 1 h periodicity over a wide range of local times, distances, and latitudes is indicative of characteristic time scales of the Kronian magnetosphere. Simple estimates of the Alfvén interhemispheric transit times in the outer Kronian magnetospheres are found to be close to 1 h, or roughly within 10% of the planetary rotation period, consistent with the idea that the observed periodic perturbations are standing Alfvén waves (Bagenal et al., 2017; Bunce et al., 2005).

The concept and theory of standing Alfvén waves were first explored by Alfvén (1942a, 1942b) and Dungey (1955) as an application of magnetohydrodynamics (MHD) to waves in a conducting medium embedded in a uniform magnetic field. Alfvén (1942b) likened the magnetic lines of force to elastic vibrating strings because of the frozen-in flux condition and named the resulting waves MHD waves. The coupling between the MHD wave modes, namely the fast (compressional) mode and the shear (Alfvén) mode, was subsequently established as a field line resonance (FLR) or, more generally, a resonant mode coupling phenomenon (Chen & Hasegawa, 1974; Radoski, 1972; Southwood, 1974; Tamao, 1965). In this paper, we treat field line resonance as any phenomenon that leads to resonant Alfvén waves, irrespective of the properties of the driver. Resonant conditions for Saturn are discussed by Glassmeier et al. (1999), concluding that the spatial structure of the resonant waves is independent of the coupling mechanism.

The problem of field line resonance is analytically tractable if evaluated using a magnetospheric box model with a uniform magnetic field. Southwood and Kivelson (1986) introduced and investigated a model with a nonuniform box-function density profile to study the effects of the Alfvén velocity gradients along the unperturbed field direction. The effects of plasma inhomogeneity along the field are particularly important for rotationally driven magnetospheres like Saturn's and Jupiter's, with dense plasma sheets centrifugally confined near the equator. Khurana and Kivelson (1989) modeled the Jovian 10–20 min ULF waves as FLR's using such a simplified hydromagnetic box model magnetosphere with a two-density plasma distribution. More recently, the hydromagnetic box model has been applied to the study of Saturn's QP60 waves (Yates et al., 2016), and Jupiter's QP 10–60 min waves (Manners & Masters, 2019). The MHD wave theory of standing Alfvén waves has also been evaluated for more complicated field geometries. Cummings et al. (1969) expressed the decoupled standing Alfvén wave equations for the toroidal and the poloidal modes in an orthogonal dipole coordinate system. Singer et al. (1981) derived and solved linearized transverse wave equations for an arbitrary field geometry, enabling numerical calculations of eigenoscillations for the toroidal and poloidal modes in arbitrary magnetic fields and plasma density distributions. A magnetic field and plasma model for Jupiter has been recently applied to investigate the field line resonances in the Jovian magnetosphere (Lysak & Song, 2020), indicating that the FLR harmonics are possible in the 10–40 min band, agreeing with the observations by Juno, Galileo, and other satellites.

Singer et al. (1981) and Warner and Orr (1979) demonstrated that a realistic field model is important for an accurate determination of resonant frequencies, especially for high invariant latitude field lines that map far into the outer magnetosphere as we discuss below. More realistic field and plasma density models have not yet been used in the modeling of the field line resonances in the Kronian magnetosphere, and it is important to do so in order to fully understand the peculiar characteristics of the QP60 waves.

2. Theory

We follow the standing wave MHD theory of Singer et al. (1981) for calculations of the field line resonances in a curvilinear coordinate system, neglecting any effects of the centrifugal or Coriolis forces. The stationary plasma conditions are justified, as the timescales of the higher ULF MHD modes are a small fraction of the planetary rotation rate (~10%) (Glassmeier et al., 1999).

From the linear MHD equations for a cold, collisionless, magnetized plasma, the wave electric field E must satisfy (ignoring the effects of a background current)

$$\frac{\partial^2 \mathbf{E}}{\partial t^2} = \mathbf{v_A} \times (\mathbf{v_A} \times (\nabla \times (\nabla \times \mathbf{E}))) \tag{1}$$

where $\mathbf{v_A} = \mathbf{B} / (\mu_0 \rho)^{1/2}$ is the Alfvén velocity, ρ is the local plasma mass density, $\mathbf{B}$ is the background field, and all vectors and differential vector operators in the wave equation depend implicitly on the coordinate along the field line. Using the Alfvén frozen-in flux condition, the wave electric field can be expressed in terms of the plasma (field) displacement $\boldsymbol{\xi}$ as

$$\mathbf{E} = -\frac{\partial \boldsymbol{\xi}}{\partial t} \times \mathbf{B} \tag{2}$$

In a uniform field embedded in cold plasma of constant density, (1) can be used to describe two uncoupled MHD wave modes: the shear Alfvén (transverse) mode, with its Poynting vector directed along **B**, and the fast (compressional) mode, with a Poynting vector angled at any direction to **B** (but parallel to the wave vector **k**). A plasma or field aligned inhomogeneity, however, couples the two modes. Assuming the longitudinal variation is $e^{im\phi}$, where ϕ is longitude and m is the azimuthal wave number, the modes decouple for special limits of m (see, Orr, 1973, for a dipole field case). Two shear Alfvén modes are then possible: one for $m = 0$ (toroidal axisymmetric b_ϕ oscillations), and the other for $m \to \infty$ (poloidal asymmetric oscillations in the meridian plane). The third uncoupled case is a fast (compressional) mode with an axisymmetric ($m = 0$) poloidal disturbance, which represents symmetric expansions and compressions of the entire magnetosphere (Orr, 1973; Radoski, 1967).

The field of a realistic magnetosphere is nonuniform. We will therefore, consider a model field with two adjacent field lines separated by a distance h_α along a unit vector $\hat{\boldsymbol{\alpha}}$ normal to the background field and by a distance h_β along a unit vector $\hat{\boldsymbol{\beta}}$ normal to both **B** and $\hat{\boldsymbol{\alpha}}$. We allow both h_α and h_β to vary along the field. We write the normal unit vector $\hat{\boldsymbol{\alpha}}$ as

$$\nabla\alpha = \hat{\boldsymbol{\alpha}} \,/\, h_\alpha \tag{3}$$

We can choose any direction $\hat{\boldsymbol{\alpha}}$ transverse to the field, but we will explicitly define our coordinate system in Section 3. Faraday's law and the Alfvén frozen-in flux condition imply that a small displacement in the $\hat{\boldsymbol{\alpha}}$ direction, ξ_α, produces a magnetic perturbation

$$\mathbf{b} = \nabla \times (\xi_\alpha \hat{\boldsymbol{\alpha}} \times \mathbf{B}) \tag{4}$$

Substituting 4 and Ampères's law in Cauchy's momentum equation (ignoring the contributions from the background currents), and assuming $\mathbf{b} \cdot \mathbf{B} = 0$ (as in Singer et al., 1981), we arrive at the wave equation for plasma (field) displacement ξ_α

$$\mu_0 \rho \frac{\partial^2 (\xi_\alpha \,/\, h_\alpha)}{\partial t^2} = \frac{1}{h_\alpha^2} \mathbf{B} \cdot \nabla \left\{ h_\alpha^2 [\mathbf{B} \cdot \nabla (\xi_\alpha \,/\, h_\alpha)] \right\} \tag{5}$$

Assuming a time dependence of the form $e^{i\omega t}$, and writing an increment along the local magnetic field **B** as ds, we rewrite 5 as a second-order partial differential equation for plasma (field) displacement ξ_α as a function of s

$$\frac{\partial^2}{\partial s^2}\left(\frac{\xi_\alpha}{h_\alpha}\right) + \frac{\partial}{\partial s}\left(ln(h_\alpha^2 B)\right)\frac{\partial}{\partial s}\left(\frac{\xi_\alpha}{h_\alpha}\right) + \frac{\mu_0 \rho \omega^2}{B^2}\left(\frac{\xi_\alpha}{h_\alpha}\right) = 0 \tag{6}$$

Once ξ_α is numerically determined using a value of the eigenfrequency, ω, that satisfies the homogeneous boundary conditions at the ionosphere ($\xi_\alpha = 0$), the magnetic perturbation, b_α, electric field perturbation E_β, and the plasma velocity, u_α, can be calculated using 4 and 2 as

$$b_\alpha = h_\alpha B \frac{\partial}{\partial s}\frac{\xi_\alpha}{h_\alpha} \tag{7}$$

$$E_\beta = -i\omega\xi_\alpha B \tag{8}$$

$$u_\alpha = i\omega\xi_\alpha \tag{9}$$

where $\hat{\boldsymbol{\beta}}$ is a unit vector perpendicular to both the unperturbed field **B** and the chosen normal vector to the field $\hat{\boldsymbol{\alpha}}$, that is,

$$\hat{\boldsymbol{\beta}} = \frac{\mathbf{B}}{|\,\mathbf{B}\,|} \times \hat{\boldsymbol{\alpha}} \tag{10}$$

We find orthogonal perturbations ξ_β, b_β, and E_α by solving 6 for a geometric scale factor, h_β, orthogonal to h_α. Equations analogous to 7 to 9 apply to the $\hat{\boldsymbol{\beta}}$ components of the perturbations.

3. Model

We use a global magnetic field of the Saturn's field (Khurana et al., 2006), based on the general deformation technique of Tsyganenko (1998); Tsyganenko (2002a, 2002b). Saturn's internal field uses magnetic moments derived from Cassini's proximal orbits (Cao et al., 2011, 2012). The field lines calculation use nominal solar wind conditions of dynamic pressure $D_P = 0.017$ nPa, $B_z = 0.1$ nT, $B_y = -0.2$ nT, and are traced using a fourth-order Runge Kutta method in a dipole centered coordinate system with x pointing toward the Sun (with Saturn's magnetic equivalent dipole being offset 0.04 R_S northward of the center of mass of Saturn).

Thanks to many Cassini plasma sheet crossings, models of plasma sheet densities and scale heights are available (Bagenal & Delamere, 2011). We use the equatorial water-group ion density profiles within the 3 –20 R_S region and use a local cubic spline to obtain the density on field lines that extend slightly beyond the modeled density profiles, crossing the equator within 20 R_S, sufficiently far out to represent regions where some of the quasiperiodic pulsations have been observed. The density variation along the field line uses an exponential scale height given by Hill and Michel (1976)

$$n(s) = n_0 \exp(-s \,/\, H)^2 \tag{11}$$

where s is distance along the field line, with $s = 0$ the maximum radial distance of the field line, the center of the plasma sheet, and we use the water-group ion scale height, H, given in Bagenal and Delamere (2011, Figure 5). We use the same equatorial plasma density profiles for the day-side and night-side, but allow the field line configuration to change with local time.

The solution of the second order partial differential equation for displacement, ξ_α (Equation 6), uses a shooting method (see Press, 2007, Section 18) with homogeneous boundary conditions in the ionosphere. We start with $\xi_\alpha = 0$ at the northern ionosphere, selecting the eigenfrequencies, ω, and the initial displacement derivatives, $d\xi/ds$, that satisfy homogeneous boundary conditions at the other end of the field line.

The local geometric scaling factors, h_α, in Equation 3 are calculated by using flux conservation along a magnetic field line. Starting from an equatorial position of the field line, two nearby field lines are mapped, displaced from the original by a finite increment along unit vectors $\hat{\boldsymbol{\alpha}}$ and $\hat{\boldsymbol{\beta}}$:

$$\hat{\boldsymbol{\alpha}} = \hat{\mathbf{b}}_\parallel \times \hat{\phi} \,/\, \left|\hat{\mathbf{b}}_\parallel \times \hat{\phi}\right| \tag{12}$$

$$\hat{\boldsymbol{\beta}} = \hat{\mathbf{b}}_\parallel \times \hat{\boldsymbol{\alpha}} \tag{13}$$

where $\hat{\mathbf{b}}_\parallel$ is a unit vector along the field line.

We verify our implementation of the model by calculating properties of the field line resonances in a purely dipolar field (Cummings et al., 1969) using the wave Equation 1 expressed in orthogonal dipole field coordinates. We also test our calculation by reproducing the known scale factors for a dipole field, that is, $h_\alpha = (rB\sin\theta)^{-1}$ and $h_\beta = r\sin\theta$.

A cross-section of a portion of the magnetosphere (field lines at invariant latitudes of 64°–73°) is visualized in Figure 1 for the day and night sides, with (a) the plasma density and (b) the Alfvén velocity color-coded along the field. The peak of the plasma density (~70 cm^{-3}) is at 4 R_S near the orbit of Enceladus, but the Alfvén velocity (especially close to the magnetic equator) varies little with x along the equator and the changes along the field are similar from one field line to the next. This will help us understand the eigenfrequencies that we discuss later.

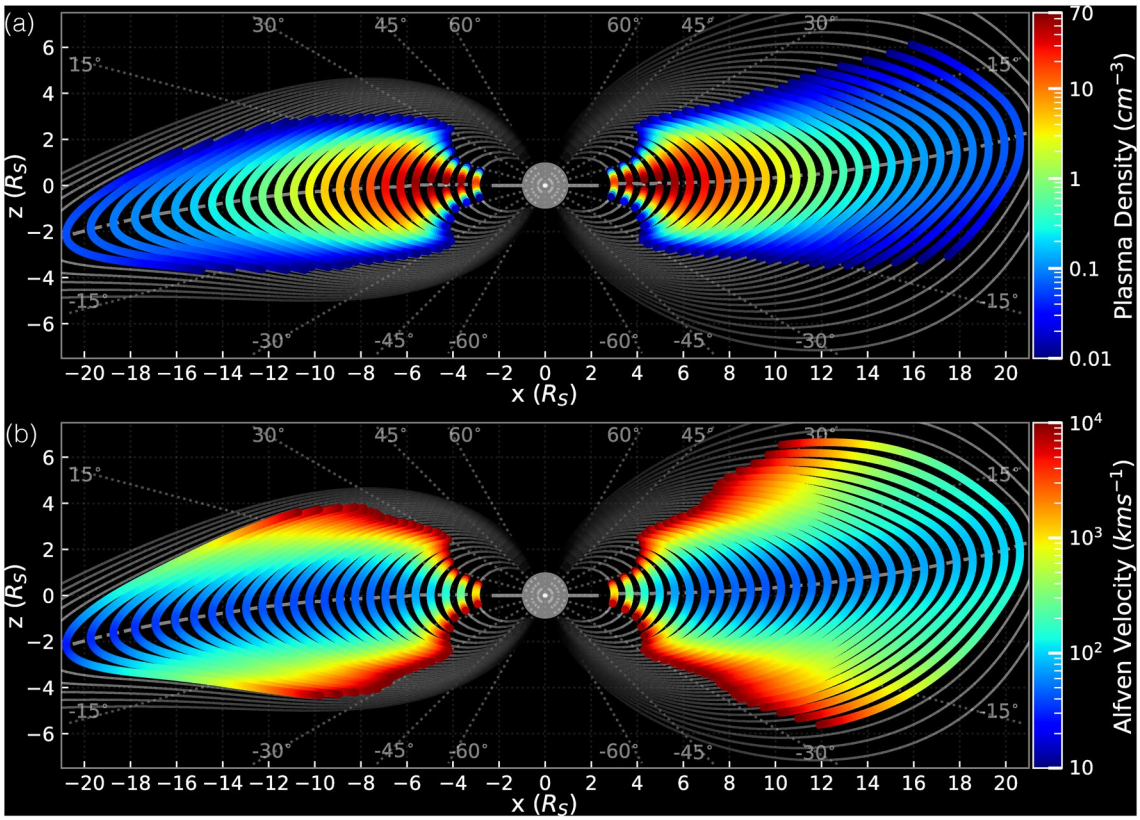

Figure 1. (a) Color plot of the plasma density (Bagenal & Delamere, 2011) in Saturn's magnetic field model (Khurana et al., 2006), visualized along field lines (solid lines, both colored and gray) of equatorial crossing distances of 3 –24 R_S. The field is in a dipole-centered coordinate system, with the x axis pointing toward the Sun. The field reversal position is marked with a thick gray dashed line. (b) Alfvén speed color plot, based upon the plasma densities and field lines visualized in Figure 1a.

4. Results

Consider a single field line that crosses the day-side equator at 20 R_S (invariant latitude 75.8°) in the field model. The wave electric field, $E_\perp$ (shown in Figure 2a) and magnetic field perturbation, $b_\perp$ (shown in Figure 2b), represent a typical form of an eigenoscillation in the outer magnetosphere of our model, calculated using the shooting-method procedure explained in the previous section. The eigenperiods of the third and fourth harmonics, 75 and 52 min, match the expected period of a QP60 event, while the eigenperiods of the second and first harmonics, 121 and 469 min, are well outside the typical QP60 range. The poloidal field displacement, $\boldsymbol{\xi}_\perp$ is shown in yellow in Figure 2c for the fourth harmonic of the same field line. Other harmonics are shown in different colors for three sufficiently separated field lines for visual clarity. As required in our wave equation solutions, the field displacement vanishes to zero at the ionosphere.

Note the magnetic field perturbation, $b_\perp$, amplitude at high latitudes (>60°) surpasses the amplitude at the equator (Figure 2b). This is consistent with the fact that QP60 pulsations are less frequently observed at the equator than at mid-to-high latitudes (Palmaerts et al., 2016; Roussos et al., 2016), perhaps because they are more readily detectable at higher latitudes where the perturbation amplitude is greater. This latitude dependence is also a feature of perturbations in a dipolar field; similar variation with latitude can be observed in the numerical results of Cummings et al. (1969) for the standing waves in Earth's dipole field, in which the perturbations at the ionosphere are 10 times larger than those at the equator. A hydromagnetic box model like the one in Southwood and Kivelson (1986) and Yates et al. (2016), in contrast, produces relatively small amplitudes of magnetic perturbations outside the plasma sheet because of the uniform magnetic field and low plasma density outside the plasma sheet.

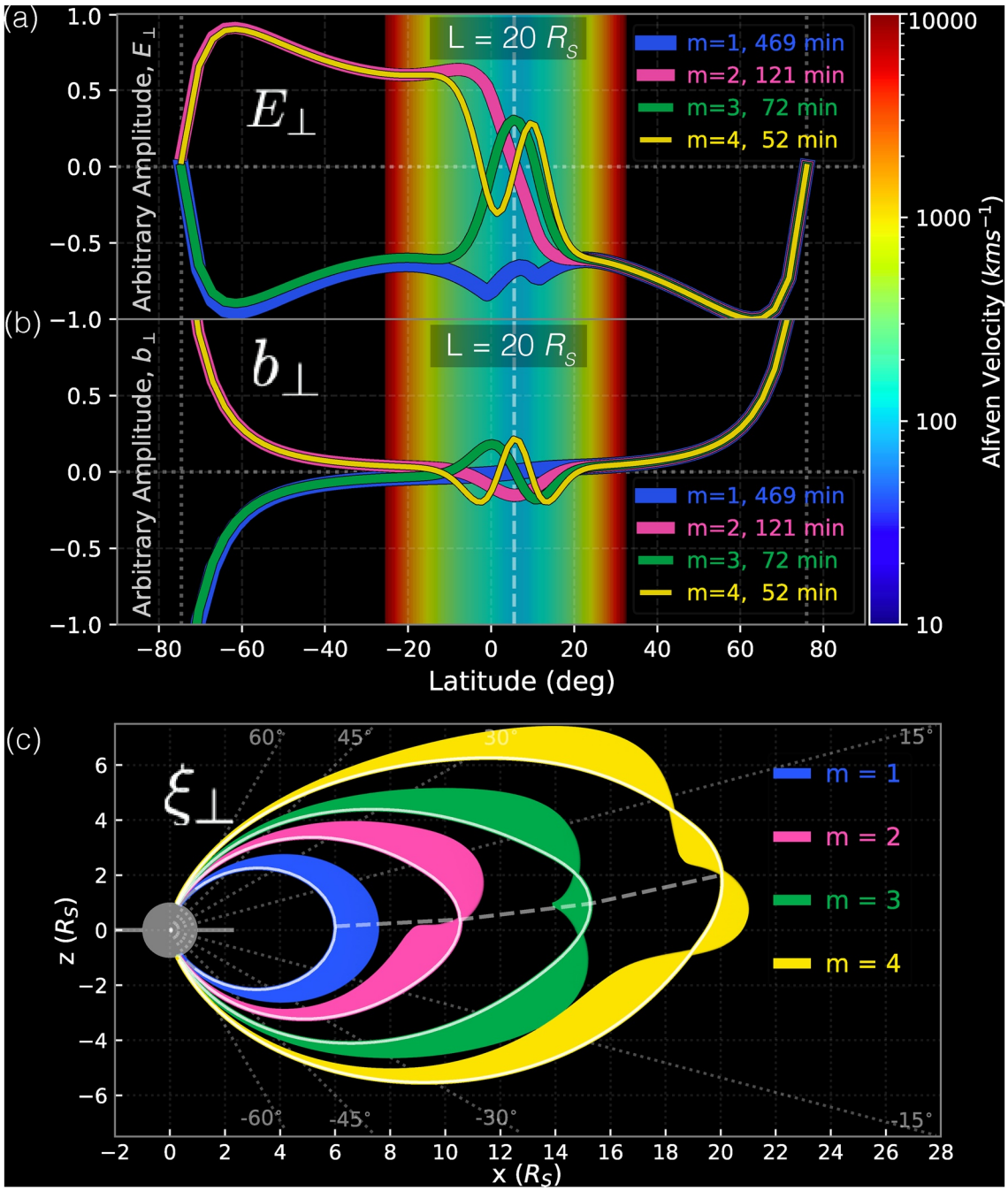

Figure 2. (a) The wave electric field, $E_\perp$, and (b) magnetic field perturbations, $b_\perp$, shown for the first four harmonics of a field line with an equatorial crossing distance of 20 R_S. The Alfvén velocity along the field line is color coded in the background. (c) Poloidal field displacement, $\boldsymbol{\xi}_\perp$, for the first four harmonics, drawn perpendicularly to four arbitrarily chosen day-side field lines that are sufficiently separated to display distinct nodal structures of the first four harmonics. All quantities in (a)–(c) are normalized to an arbitrary amplitude of 1.

The nodes and the local peaks of field perturbations occur within the denser region of the plasma sheet (Figure 2a). The exception to this is the fundamental mode, which does not have any nodes beyond the ionosphere, and is less sensitive to the ambient plasma. The close spacing of the nodes of the higher harmonics near the equator (or equivalently, the short parallel wavelength of the perturbations) can be understood by evaluating the radius of curvature, R_c, which for slow changes of the field magnitude, can be approximated (see Riley et al., 2006) as

$$\frac{\hat{\mathbf{n}}}{R_c} \approx -\frac{(\mathbf{B}\cdot\nabla)\mathbf{B}}{B^2} \tag{14}$$

Let's consider a small perpendicular perturbation, $\mathbf{b}_\perp$, in the $\hat{\boldsymbol{\alpha}}$ direction. Since $(\hat{\mathbf{B}}\cdot\nabla) = \partial / \partial s$ for a field-aligned coordinate system, we can rewrite 14 as

$$\frac{\hat{\mathbf{n}}}{R_c} \approx -\frac{\partial}{\partial s}\left(\frac{\mathbf{B}+\mathbf{b}}{|\,\mathbf{B}+\mathbf{b}\,|}\right) \approx -\frac{\hat{\mathbf{n}}}{R_{c,B}} - \frac{\partial}{\partial s}\left(\frac{b_\alpha\hat{\boldsymbol{\alpha}}}{h_\alpha B}\right) \approx -\frac{\partial}{\partial s}\left(\frac{b_\alpha\hat{\boldsymbol{\alpha}}}{h_\alpha B}\right) \tag{15}$$

where we neglected the contribution of the perturbation to the total field strength in the denominator. We substitute the expression for b_α (7) for the last term in 15, assuming the geometric scale factor, h_α, varies negligibly near the equator. Since the radius of curvature of the background field, $R_{c,B}$, is big, and $\hat{\boldsymbol{\alpha}}$ changes slowly with s, we then get

$$\frac{\hat{\mathbf{n}}}{R_c} \approx -\hat{\boldsymbol{\alpha}}\frac{\partial}{\partial s}\left(\frac{b_\alpha}{h_\alpha B}\right) = -\hat{\boldsymbol{\alpha}}\frac{\partial^2}{\partial s^2}\left(\frac{\xi_\alpha}{h_\alpha}\right) \tag{16}$$

Noting that the second term in 6 scales like variations in the background field and is small above the fundamental

$$\frac{\hat{\mathbf{n}}}{R_c} = \left(\frac{\hat{\boldsymbol{\alpha}}}{h_\alpha}\right)\frac{\omega^2}{v_A^2}\xi_\alpha \tag{17}$$

where b_α is a field perturbation in the $\hat{\boldsymbol{\alpha}}$ direction and we assumed the orientation of the background field to be changing slowly at the equator.

Therefore, a small radius of curvature in a region of low Alfvén velocity implies that the perturbation reverses sign over a comparatively short range of s, and that the local wavelength of the perturbation field is small.

This explains the close spacing of the nodes of the perturbation near the equator, but does not account for the high perturbation amplitudes near the plasma sheet and in the tenuous high-latitude regions. High amplitudes closer to the ionosphere can be viewed as an effect of a curvilinear field geometry, where the field strength becomes large close to the planet. Even small reorientation of a strong field can create a significant perturbation field. As seen in Equation 7, the magnetic perturbation amplitude, b_α, is proportional to the magnitude of the unperturbed field, $|\mathbf{B}|$.

Because we use a realistic model of Saturn's magnetic field, the field lines of the same invariant latitude map differently from ionosphere to equator in the day-side and night-side meridians (see Figures 1a and 1b). We calculate the resonant periods separately for the day-side and night-side field lines (Figures 3a and 3b, respectively) for both the toroidal and the poloidal modes. Only the fundamental gives values that notably differ between the two modes, similar to the findings of Orr and Matthew (1971), but in the outer magnetosphere, those periods greatly exceed 1 h. Consequently, we will not distinguish between the toroidal and the poloidal modes.

Field line resonances in substantial regions of the outer magnetosphere (invariant latitudes of 72°–76° on the day-side, and 72°–74° on the night-side) have periods that vary little with equatorial crossing distance for the harmonics above the fundamental. The third (odd) and the fourth (even) harmonics oscillate at close to a 60 min period in this region. The field lines with 60 min resonances map to equatorial radii of 10–20 R_S. Notably, the resonant periods on the night-side start to increase sharply past 74° invariant latitude. Since the field is highly stretched on the night side, the field lines map into a region outside the validity of the plasma sheet models of Bagenal and Delamere (2011). A model of the plasma sheet density valid at larger distances might reveal a larger region for the 1 h eigenoscillations on the night side. The day-side magnetosphere, on the other hand, is compressed, and the resonant periods remain roughly constant for field lines of higher invariant latitudes, even close to the magnetopause.

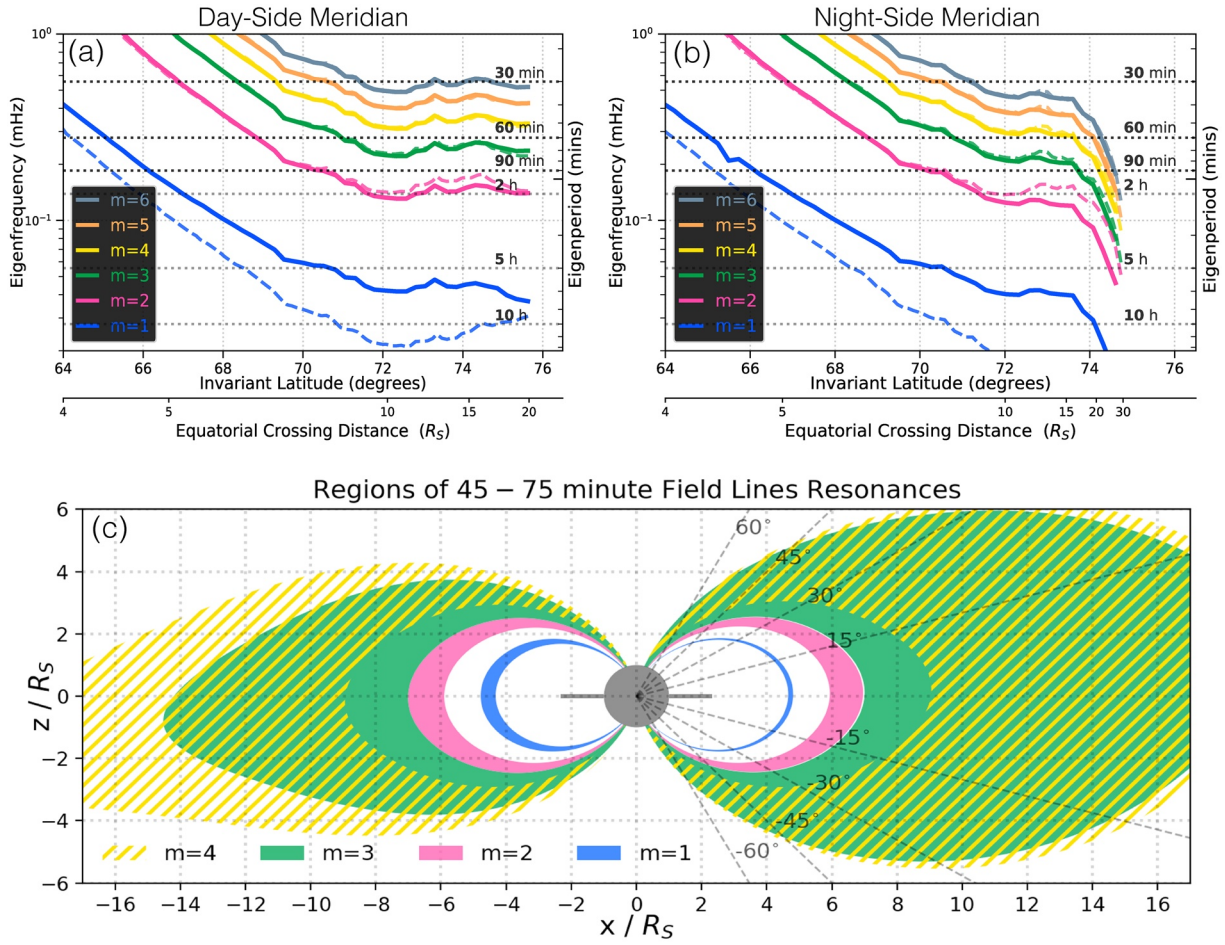

Figure 3. (a) Eigenfrequencies for the first six toroidal (solid) and poloidal (dashed) modes for varying invariant latitudes of field lines in the day side of Saturn's magnetosphere. (b) Same as (a), but for the night-side meridian. (c) Regions of 45–75 min field line resonances for the first four modes, shown for the day and night side meridian planes.

The regions in which field lines resonate with periods of 45–75 min are indicated in 3c. Only the third and the fourth harmonics resonate at ~1 h eigenperiods (45–75 min) in the outer magnetosphere (10 –20 R_S in radial distance from the planet), with the fundamental and the second harmonic resonating close to this period only in very narrow ranges close to the planet. If we compare our results to those for a purely dipolar field embedded in the same plasma distribution, it becomes apparent that a realistic field model is important for producing these large regions of field lines resonances with 1-h periodicities (see Supplementary Figure S1). The eigenperiods in the dipole model decrease continuously with L, and beyond ~15 R_S do not fall in the required 45–75 min range. Saturn's field becomes decreasingly dipolar beyond ~10 R_S from the planet, and the stretched-out field geometry produces a roughly constant eigenperiod in the outer magnetosphere (at least up to 20 R_S in our model). Thus, neither a hydromagnetic box model nor a dipole field provides a valid model of the periodic phenomena observed in Saturn's magnetosphere.

5. Conclusion

Using the approach introduced by Singer et al. (1981), we have calculated the resonant frequencies of MHD waves in regions within ~20 R_S of Saturn using realistic models of the magnetic field (Khurana et al., 2006) and the plasma density (Bagenal & Delamere, 2011). We find that field line resonances can produce the quasiperiodic ~60 min pulsations reported in particle and field data. As contrasted with the standing wave periods calculated in a hydromagnetic box model, the eigenperiods matching the observations the closest are produced by the third (odd) and fourth (even) harmonics, rather than the second (even) mode (Yates

et al., 2016). The period of the fundamental is comparable to the rotational rate of the planet, prohibiting the development of such long-period Alfvén standing modes (Glassmeier et al., 2004). Higher harmonics may also be present in Saturn's magnetosphere but the wave power at the higher frequencies is probably not observable.

We have established that a realistic magnetic field model is important for obtaining quantitative eigenperiods of field line resonances, especially in the outer magnetosphere. Even the combination of a realistic plasma density distribution and a purely dipolar model produces model eigenperiods that continue to increase with L beyond roughly 15 R_S, inconsistent with the widespread appearance of fluctuations in the ~60 min range. Our implementation of a realistic field model reveals that there are large regions in the outer magnetosphere (10–20 R_S) in which resonances have eigenperiods in the 45–75 min range, even as the flux tubes become long compared with the height of the high density region near the equator. We would expect to identify fewer pulsations at latitudes of 15°–60°. At the equator, the plasma sheet is dense, and the local peaks are confined to a narrow region of roughly ±15°. Many QP60 pulsations have been detected very close to the equator (Palmaerts et al., 2016), but the closeness of the magnetic field perturbation nodes may make it difficult to distinguish between the odd and even modes (Figure 2b).

We were limited to considering field lines that cross the equator within 20 R_S by the restricted distance range of the plasma density model; it would be informative to extend the plasma density model to establish if eigenperiods of 1 h extend into the outer magnetosphere beyond 20 R_S. Our model assumes wave perturbations transverse to the background field and a perfectly conducting ionosphere (i.e. $E_\perp = 0$ at the field line boundaries). These assumptions can be justified. Most of the QP60 pulsations map to the auroral zone on closed field lines (Roussos et al., 2016). The highly conducting auroral regions of the ionosphere satisfy our $E_\perp$~0 condition most closely and should provide sufficiently good reflection for the development of a standing wave. Nevertheless, the fact that these Alfvén waves come in 4–6 h wave trains implies a dissipation mechanism, and wave damping by a less than perfectly conducting ionosphere could account for the wave decay. However, a quantitative model of wave decay also requires knowledge of the time-variation of the driving source, which is not readily characterized.

Our work also neglected the effects of Saturn's rotating plasma (similar to Glassmeier et al., 1989). We believe this approximation is valid for the higher resonance modes, for which the plasma is quasistationary relative to the MHD wave timescales. An analytical treatment of MHD perturbations in a rotating plasma by Ferrière et al. (1999) shows that the stability of the Alfvén modes either remains unchanged or increases with the inclusion of the Coriolis force, albeit for constant background parameters along the field. Furthermore, the estimates of magnetic Rossby numbers by Glassmeier et al. (1999) show that rotation has no significant impact on any resonant coupling at Jupiter or Saturn.

Although the classical mechanism of field line resonances seems plausible, it is challenging to identify the energy source that excites the oscillations. Any phenomenon that disturbs a quasiequilibrium state of the magnetosphere can, in principle, excite field line resonances. Possible sources include such external disturbances as interplanetary shocks or pressure fronts, boundary oscillations driven by the Kelvin-Helmholtz instability or magnetic reconnection, and internal disturbances such as those arising from reconnection in the plasma sheet. Because the third and fourth harmonics map to field lines close to the magnetopause, the possibility of the waves being driven externally by the solar wind buffeting (Mathie & Mann, 2000), or alternatively, by the Kelvin Helmholtz instability at the magnetopause boundary (Fujita et al., 1996) becomes an attractive suggestion. Resonant mode coupling between fast mode magnetopause surface waves and the local Alfvén waves has been previously reported in Saturn's magnetosphere – transverse Alfvén perturbations have been observed 2 h after an observation of Kelvin Helmholtz waves of the same period, albeit of 23 min periodicity, not 1 h (Cramm et al., 1998; Lepping et al., 1981). A proposed explanation for the source of these waves, at least on the day side, is magnetodisk reconnection (Guo et al., 2018). Guo et al. (2018) observed QP60 events for 14 h during a reconnection event, and the energy flux has been estimated to be high enough to power aurorea (~2.6 mWm^{-2}). If the QP60 events, including the auroral pulsations, are driven by magnetodisc or magnetopause reconnection, we could estimate the energy input into the FLR's and model their dissipation.

Further data analysis of the distribution, magnitude, and symmetry of the quasiperiodic waves will show if their properties match those of our modeled third to fifth harmonics. Particularly, we would expect to see more pulsations at magnetic latitudes of 60° and higher, where the magnetic field perturbation amplitudes surpass those at the equatorial plasma sheet. As seen in Figure 3, the third to fifth mode with a period in the critical range can develop through much of the outer magnetosphere.

Data Availability Statement

The realistic field model for Saturn was provided by Krishan K. Khurana, and is available on the open-access repository Zenodo (Khurana, 2020).The software code used to model the standing waves, interact with the magnetic field model, and generate the figures in this paper is available as a packaged release called AlfvenWaver on GitHub and Zenodo (Rusaitis, 2020).

Acknowledgments
The authors are grateful to Robert Strangeway for useful discussions on the subject during many weekly meetings. The realistic field model for Saturn was provided by Krishan K. Khurana, and is available on the open-access repository Zenodo (Khurana, 2020).

References

Alfvén, H. (1942a). Existence of electromagnetic-hydrodynamic waves. *Nature*, *150*, 405–406. https://doi.org/10.1038/150405d0

Alfvén, H. (1942b). On the existence of electromagnetic-hydrodynamic waves. *Arkiv för Matematik, Astronomi och Fysik*, *29B*, 1–7.

Bader, A., Badman, S. V., Yao, Z. H., Kinrade, J., & Pryor, W. R. (2019). Observations of continuous quasiperiodic auroral pulsations on Saturn in high time-resolution UV auroral imagery. *Journal of Geophysical Research: Space Physics*, *124*, 2451–2465. https://doi.org/10.1029/2018JA026320

Bagenal, F., Adriani, A., Allegrini, F., Bolton, S. J., Bonfond, B., Bunce, E. J., et al. (2017). Magnetospheric science objectives of the Juno mission. *Space Science Reviews*, *213*, 219–287. https://doi.org/10.1007/s11214-014-0036-8

Bagenal, F., & Delamere, P. A. (2011). Flow of mass and energy in the magnetospheres of Jupiter and Saturn. *Journal of Geophysical Research*, *116*, A05209. https://doi.org/10.1029/2010JA016294

Bunce, E. J., Cowley, S. W. H., & Milan, S. E. (2005). Interplanetary magnetic field control of Saturn's polar cusp aurora. *Annales Geophysicae*, *23*, 1405–1431. https://doi.org/10.5194/angeo-23-1405-2005

Bunce, E. J., Grodent, D. C., Jinks, S. L., Andrews, D. J., Badman, S. V., Coates, A. J., et al. (2014). Cassini nightside observations of the oscillatory motion of Saturn's northern auroral oval. *Journal of Geophysical Research: Space Physics*, *119*, 3528–3543. https://doi.org/10.1002/2013JA019527

Cao, H., Russell, C. T., Christensen, U. R., Dougherty, M. K., & Burton, M. E. (2011). Saturn's very axisymmetric magnetic field: No detectable secular variation or tilt. *Earth and Planetary Science Letters*, *304*, 22–28. https://doi.org/10.1016/j.epsl.2011.02.035

Cao, H., Russell, C. T., Wicht, J., Christensen, U. R., & Dougherty, M. K. (2012). Saturn's high degree magnetic moments: Evidence for a unique planetary dynamo. *Icarus*, *221*, 388–394. https://doi.org/10.1016/j.icarus.2012.08.007

Carbary, J. F., Kurth, W. S., & Mitchell, D. G. (2016). Short periodicities in low-frequency plasma waves at Saturn: Short periodicities at Saturn. *Journal of Geophysical Research: Space Physics*, *121*, 6562–6572. https://doi.org/10.1002/2016JA022732

Chen, L., & Hasegawa, A. (1974). A theory of long-period magnetic pulsations: 1. Steady state excitation of field line resonance. *Journal of Geophysical Research*, *79*, 1024–1032. https://doi.org/10.1029/JA079i007p01024

Cramm, R., Glassmeier, K.-H., Stellmacher, M., & Othmer, C. (1998). Evidence for resonant mode coupling in Saturn's magnetosphere. *Journal of Geophysical Research*, *103*, 11951–11960. https://doi.org/10.1029/98JA00629

Cummings, W. D., O'Sullivan, R. J., & Coleman, P. J. (1969). Standing Alfvén waves in the magnetosphere. *Journal of Geophysical Research*, *74*, 778–793. https://doi.org/10.1029/JA074i003p00778

Dungey, J. W. (1955). Electrodynamics of the outer atmosphere. *Physics of the ionosphere* (p. 229). London: The Physical Society.

Ferrière, K. M., Zimmer, C., & Blanc, M. (1999). Magnetohydrodynamic waves and gravitational/centrifugal instability in rotating systems. *Journal of Geophysical Research*, *104*, 17335–17356. https://doi.org/10.1029/1999JA900167

Fujita, S., Glassmeier, K.-H., & Kamide, K. (1996). MHD waves generated by the Kelvin-Helmholtz instability in a nonuniform magnetosphere. *Journal of Geophysical Research*, *101*, 27317–27325. https://doi.org/10.1029/96JA02676

Glassmeier, K.-H., Klimushkin, D., Othmer, C., & Mager, P. (2004). ULF waves at Mercury: Earth, the giants, and their little brother compared. *Advances in Space Research*, *33*, 1875–1883. https://doi.org/10.1016/j.asr.2003.04.047

Glassmeier, K.-H., Ness, N. F., Acuña, M. H., & Neubauer, F. M. (1989). Standing hydromagnetic waves in the Io plasma torus: Voyager 1 observations. *Journal of Geophysical Research*, *94*, 15063. https://doi.org/10.1029/JA094iA11p15063

Glassmeier, K.-H., Othmer, C., Cramm, R., Stellmacher, M., & Engebretson, M. (1999). Magnetospheric field line resonances: A comparative planetology approach. *Surveys in Geophysics*, *20*, 61–109. https://doi.org/10.1023/A:1006659717963

Guo, R. L., Yao, Z. H., Wei, Y., Ray, L. C., Rae, I. J., Arridge, C. S., et al. (2018). Rotationally driven magnetic reconnection in Saturn's dayside. *Nature Astronomy*, *2*, 640–645. https://doi.org/10.1038/s41550-018-0461-9

Hill, T. W., & Michel, F. C. (1976). Heavy ions from the Galilean satellites and the centrifugal distortion of the Jovian magnetosphere. *Journal of Geophysical Research*, *81*, 4561–4565. https://doi.org/10.1029/JA081i025p04561

Khurana, K. K. (2020). KMAG: Kronian magnetic field model. *American Geophysical Union, Fall Meeting 2016* (pp. 12–16), San Francisco, CA: Zenodo. https://doi.org/10.5281/ZENODO.4080294

Khurana, K. K., Arridge, C. S., Schwarzl, H., & Dougherty, M. K. (2006). A model of Saturn's magnetospheric field based on latest Cassini observations. *AGU Spring Meeting Abstracts, 2007* (P44A–-1).

Khurana, K. K., & Kivelson, M. G. (1989). Ultralow frequency MHD waves in Jupiter's middle magnetosphere. *Journal of Geophysical Research*, *94*, 5241. https://doi.org/10.1029/JA094iA05p05241

Kleindienst, G., Glassmeier, K.-H., Simon, S., Dougherty, M. K., & Krupp, N. (2009). Quasiperiodic ULF-pulsations in Saturn's magnetosphere. *Annales Geophysicae*, *27*, 885–894. https://doi.org/10.5194/angeo-27-885-2009

Lepping, R. P., Burlaga, L. F., & Klein, L. W. (1981). Surface waves on Saturn's magnetopause. *Nature*, *292*, 750–753. https://doi.org/10.1038/292750a0

Lysak, R. L., & Song, Y. (2020). Field line resonances in Jupiter's magnetosphere. *Geophysical Research Letters*, *47*, e2020GL089473. https://doi.org/10.1029/2020GL089473
Manners, H., & Masters, A. (2019). First evidence for multiple-harmonic standing Alfvén waves in Jupiter's equatorial plasma sheet. *Geophysical Research Letters*, *46*, 9344–9351. https://doi.org/10.1029/2019GL083899
Mathie, R. A., & Mann, I. R. (2000). Observations of Pc5 field line resonance azimuthal phase speeds: A diagnostic of their excitation mechanism. *Journal of Geophysical Research*, *105*, 10713–10728. https://doi.org/10.1029/1999JA000174
Menietti, J. D., Palmaerts, B., Zahlava, J., Averkamp, T. F., Groene, J. B., & Kurth, W. S. (2020). Quasiperiodic Saturn auroral hiss observed during a Cassini proximal orbit. *Journal of Geophysical Research: Space Physics*, *125*. https://doi.org/10.1029/2019JA027338
Mitchell, D. G., Carbary, J., Bunce, E., Radioti, A., Badman, S., Pryor, W., et al. (2016). Recurrent pulsations in Saturn's high latitude magnetosphere. *Icarus*, *263*, 94–100. https://doi.org/10.1016/j.icarus.2014.10.028
Mitchell, D. G., Krimigis, S. M., Paranicas, C., Brandt, P., Carbary, J., Roelof, E., et al. (2009a). Recurrent energization of plasma in the midnight-to-dawn quadrant of Saturn's magnetosphere, and its relationship to auroral UV and radio emissions. *Planetary and Space Science*, *57* 1732–1742. https://doi.org/10.1016/j.pss.2009.04.002
Mitchell, D. G., Kurth, W. S., Hospodarsky, G. B., Krupp, N., Saur, J., Mauk, B. H., et al. (2009b). Ion conics and electron beams associated with auroral processes on Saturn. *Journal of Geophysical Research*, *114*, A02212. https://doi.org/10.1029/2008JA013621
Orr, D. (1973). Magnetic pulsations within the magnetosphere: A review. *Journal of Atmospheric and Terrestrial Physics*, *35*, 1–50. https://doi.org/10.1016/0021-9169(73)90214-6
Orr, D., & Matthew, J. A. D. (1971). The variation of geomagnetic micropulsation periods with latitude and the plasmapause. *Planetary and Space Science*, *19*, 897–905. https://doi.org/10.1016/0032-0633(71)90141-3
Palmaerts, B., Roussos, E., Krupp, N., Kurth, W., Mitchell, D., & Yates, J. (2016). Statistical analysis and multi-instrument overview of the quasi-periodic 1-hour pulsations in Saturn's outer magnetosphere. *Icarus*, *271*, 1–18. https://doi.org/10.1016/j.icarus.2016.01.025
Press, W. H., Teukolsky, S. A., Vetterling, W. T., & Flannery, B. P. (Ed.), (2007). *Numerical recipes: The art of scientific computing* (3rd ed., p. 1256). New York, NY: Cambridge University Press. http://www.cambridge.org/numericalrecipes
Radoski, H. R. (1967). A note on oscillating field lines. *Journal of Geophysical Research*, *72*, 418. https://doi.org/10.1029/JZ072i001p00418
Radoski, H. R. (1972). The effect of asymmetry on toroidal hydromagnetic waves in a dipole field. *Planetary and Space Science*, *20*, 1015–1023. https://doi.org/10.1016/0032-0633(72)90212-7
Riley, K. F., Hobson, M. P., & Bence, S. J. (2006). *Mathematical Methods for Physics and Engineering* (3rd ed.). Cambridge, MA: Cambridge University Press. https://doi.org/10.1017/CBO9780511810763
Roussos, E., Krupp, N., Mitchell, D., Paranicas, C., Krimigis, S., Andriopoulou, M., et al. (2016). Quasi-periodic injections of relativistic electrons in Saturn's outer magnetosphere. *Icarus*, *263*, 101–116. https://doi.org/10.1016/j.icarus.2015.04.017
Rusaitis, L. (2020). *AlfvenWaver*. Zenodo. https://doi.org/10.5281/ZENODO.4116492
Schardt, A. W., Kurth, W. S., Lepping, R. P., & Maclennan, C. G. (1985). Particle acceleration in Saturn's outer magnetosphere: In memoriam Alois Schardt. *Journal of Geophysical Research*, *90* 8539. https://doi.org/10.1029/JA090iA09p08539
Singer, H. J., Southwood, D. J., Walker, R. J., & Kivelson, M. G. (1981). Alfven wave resonances in a realistic magnetospheric magnetic field geometry. *Journal of Geophysical Research*, *86*, 4589–4596. https://doi.org/10.1029/JA086iA06p04589
Southwood, D. J. (1974). Some features of field line resonances in the magnetosphere. *Planetary and Space Science*, *22*, 483–491. https://doi.org/10.1016/0032-0633(74)90078-6
Southwood, D. J., & Kivelson, M. G. (1986). The effect of parallel inhomogeneity on magnetospheric hydromagnetic wave coupling. *Journal of Geophysical Research*, *91*, 6871. https://doi.org/10.1029/JA091iA06p06871
Tamao, T. (1965). Transmission and coupling resonance of hydromagnetic disturbances in the non-uniform Earth's magnetosphere. *Science reports of the Tohoku University. Ser. 5, Geophysics*, *17*, 43–70.
Tsyganenko, N. A. (1998). Modeling of twisted/warped magnetospheric configurations using the general deformation method. *Journal of Geophysical Research*, *103*, 23551–23563. https://doi.org/10.1029/98JA02292
Tsyganenko, N. A. (2002a). A model of the near magnetosphere with a dawn-dusk asymmetry 1. Mathematical structure. *Journal of Geophysical Research*, *107*. https://doi.org/10.1029/2001JA000219
Tsyganenko, N. A. (2002b). A model of the near magnetosphere with a dawn-dusk asymmetry 2. Parameterization and fitting to observations. *Journal of Geophysical Research*, *107*(A8). https://doi.org/10.1029/2001JA000220
Warner, M., & Orr, D. (1979). Time of flight calculations for high latitude geomagnetic pulsations. *Planetary and Space Science*, *27*, 679–689. https://doi.org/10.1016/0032-0633(79)90165-X
Yates, J. N., Southwood, D. J., Dougherty, M. K., Sulaiman, A. H., Masters, A., Cowley, S. W. H., et al. (2016). Saturn's quasiperiodic magnetohydrodynamic waves. *Geophysical Research Letters*, *43*, 11102–11111. https://doi.org/10.1002/2016GL071069